IEEE Access
Multidisciplinary ⋮ Rapid Review ⋮ Open Access Journal

Received 23 November 2023, accepted 9 December 2023, date of publication 18 December 2023,
date of current version 22 December 2023.

Digital Object Identifier 10.1109/ACCESS.2023.3343868

RESEARCH ARTICLE

Scattered Field Calculation From Microstrip Arrays Using the Combination of Discrete Bodies of Revolution and Domain Decomposition Methods

HOSSEIN MOHAMMADZADEH, ABOLGHASEM ZEIDAABADI NEZHAD, (Member, IEEE), AND ZAKER HOSSEIN FIROUZEH

Department of Electrical and Computer Engineering, Isfahan University of Technology, Isfahan 84156-83111, Iran

Corresponding author: Abolghasem Zeidaabadi Nezhad (zeidabad@iut.ac.ir)

ABSTRACT This paper analyzes electromagnetic scattering from a microstrip array with a homogeneous dielectric substrate in two symmetry cases. In the first case, the entire structure has discrete rotational symmetry, and the discrete bodies of revolution method is employed for a comprehensive analysis. In the second case, the ground and substrate have discrete rotational symmetry, whereas the patches and feeding lines do not. Therefore, the discrete bodies of revolution method is used to analyze the ground and substrate, the traditional moment method is applied to the patches and feeding lines connected to them, and the domain decomposition method combines the results obtained from these two solutions. As a result, the discrete bodies of revolution method is applied only to one sector of the microstrip array, which reduces the memory requirements and computational time in comparison with the traditional moment method. Consequently, for a structure with N_s symmetric sectors and the total number of unknowns N, the memory requirements and simulation time are reduced by factors of N_s^2 and N_s^3, respectively, in comparison to the traditional moment method. Finally, numerical results are presented to validate the accuracy and efficiency of the proposed method. The results are compared with those obtained from commercial FEKO software and the traditional moment method to show how the proposed method reduces computation time and memory requirements.

INDEX TERMS Discrete bodies of revolution (DBOR), domain decomposition method (DDM), traditional method of moment (MoM).

I. INTRODUCTION

Various methods are available for calculating the scattering of electromagnetic waves, including asymptotic and full-wave methods. Asymptotic methods like Physical Optics (PO) and Geometrical Optics (GO) are efficient, but they have weak accuracy when dealing with structures that have dimensions smaller than the wavelength, especially in structures that include dielectrics. PO and GO are sufficiently accurate at high frequencies due to the shallow penetration depth of electromagnetic fields and the consideration of structural details. However, PO and GO fail to provide satisfactory solutions at low frequencies, where the penetration depth is significantand the structural details are comparable with the wavelength. Therefore, full-wave methods are primarily employed to achieve the desired accuracy in scattering field calculations. Several full-wave methods can be utilized for calculating the scattered field [1], [2], [3], [4], [5].

Because the electromagnetic scattering fields for a homogeneous structure can be obtained by calculating the surface current density of the structure, it is advantageous to use methods based on a surface mesh. Methods based on surface meshing, such as the method of moment (MoM), have significantly fewer unknowns compared to methods based on volume meshing, such as the Finite Difference Time Domain (FDTD) and Finite Element Method (FEM) [6], [7], [8], [9].

The associate editor coordinating the review of this manuscript and approving it for publication was Guido Lombardi.

In the MoM, each observational element is interconnected with every source element. Hence, for the number of unknowns N, the complexity order of solving the matrix equation using conventional methodologies such as Gaussian elimination is $O(N^2)$ for memory and $O(N^3)$ for computation time [6], [9], [10]. Consequently, as the size of the structure increases, the calculation time and required memory drastically increase. An approximation can be used to address this issue, and observation and source elements are boxed and grouped in several different levels. Instead of calculating the relationship between each element of observation and source, it is sufficient to determine the relationship between elements within each box. Calculating the relationship between the boxes can solve the problem using an iterative method. This technique is known as the Multilevel Fast Multipole Method (MLFMM) [6], [9]. The MLFMM significantly reduces the required memory to an order of $O(N \log N)$, substantially reducing calculation time and memory requirements compared to the traditional MoM.

However, the MLFMM has some drawbacks. In structures incorporating dielectrics, the wavelength inside the dielectric is lower than that in free space, leading to reduced box dimensions and an increased number of boxes. This increase in the number of boxes decreases the convergence rate in problem-solving and significantly prolongs calculation time. Additionally, in the case of monostatic scattering, the iterative nature of the method necessitates solving the problem again for each radiation angle, further increasing calculation time [11].

Several methods have been proposed in recent years to overcome these limitations, most of which simplify the problem by applying approximations [12], [13], [14], [15], [16]. One such method is the finite array approximation with an infinite periodic array, which examines a single cell of the structure and assumes an infinite number of similar single cells in the array. While these methods offer high-speed solutions, they do not consider the edge effects of the finite array, resulting in inaccurate scattering fields at non-perpendicular angles. To achieve calculations with high accuracy and speed using low memory, utilizing the traditional MoM and exploiting the existing symmetry in the problem is recommended simultaneously.

One technique to reduce memory requirements in the FEM method is the use of the discrete bodies of revolution (DBOR) method, which has been employed in recent years to solve electromagnetic problems with discrete rotational symmetry [17], [18]. If the structure of the rotating body is discrete, calculations can be reduced proportionally to the number of discrete parts. Therefore, the more discrete parts with rotational symmetry, the greater the reduction in calculations. However, due to the volume meshing nature of the FEM method, it is not advisable to use this method alone to analyze the scattered fields of the structures. This method is mostly used with other methods to analyze the scattering field of complex structures, such as the air intake duct of a fighter engine [17], [19]. Hence, solving the problem using integral equation methods with surface meshing is preferable.

The use of the DBOR method in solving problems with integral equations has gained attention in recent years [20], [21], [22], [23], [24], [25], [26]. To employ this method, it is necessary to have sectors in the structure that are completely similar in terms of element shape, current distribution, and distance between elements. The formation of the block circulant matrix in the matrix equations of the DBOR method requires these structural characteristics. In this method, for an array with N_s symmetrical sectors, the required memory and calculation time are reduced by the ratio of N_s^2 and N_s^3, respectively [20], [22], [23], [24], [25], [26]. However, in practice, lower ratios are achieved due to overhead calculations in the implementation of the proposed method. Nevertheless, up until now, the DBOR method has only been utilized to calculate the field scattering of metallic structures [20], [22], [23], [24], [25], [26]. In [21], the problem of scattering from a structure with a dielectric material is solved. However, for two reasons, this paper's proposed method is ineffective. First, this paper employs the volume equivalence theorem (VET) and volume meshing for dielectric modeling. Second, the analysis is limited to a cylindrical waveguide, and the cylindrical waveguide dyadic Green's function is used to analyze the problem.

This paper aims to analyze the homogeneous scattering problems for microstrip arrays with discrete rotating symmetrical sectors, such as microstrip antenna arrays and frequency selective surface (FSS) absorbers. The microstrip arrays utilize a homogeneous dielectric substrate. Therefore, the description of the surface integral equations and the formulation of PMCHW (Poggio, Miller, Chang, Harrington, Wu) are used. It is important to note that the number of arrays with feeding lines and patches exhibiting discrete rotational symmetry is limited. Therefore, in this paper, we utilize the Domain Decomposition Method (DDM) [27] to enhance the capacity of the proposed method in analyzing a more significant number of structures.

The rest of the paper is organized as follows. The analysis of the scattering problems is described in Section II. Applying the DBOR method to integral equations is expressed in Section III. Combining the DBOR method and the traditional MoM by DDM is represented in Section IV. The accuracy and validity of the proposed method are examined in Section V, where it is compared with commercial FEKO software and the traditional MoM. Concluding remarks are given in Section VI.

II. ANALYSIS OF SCATTERING PROBLEMS WITH DISCRETE ROTATIONAL SYMMETRY

Analyzing wave scattering through full-wave methods necessitates significant memory usage and time consumption. However, by leveraging the problem's symmetry and employing the DBOR method, it is possible to streamline the analysis and reduce the computational workload. Consequently, the DBOR method simplifies structures exhibiting such

symmetry, allowing for analyzing only one symmetry sector using the abovementioned method. The subsequent sections outline the process of problem-solving and applying the DBOR method to it.

A. ANALYSIS OF SCATTERING PROBLEMS USING THE MOM

Numerous numerical methods exist for solving scattering problems, including those based on volume and surface meshing. In wave scattering problems, the area under consideration is often extensive. Consequently, employing volumetric meshing methods increases the number of unknowns, resulting in slower calculations and greater computational memory requirements. To address these challenges, methods based on surface meshing are commonly utilized. One such approach for solving scattering problems involves formulating integral equations and employing the MoM to solve them. Obtaining the matrix representation of these equations using the MoM after formulating the integral equations is necessary to accomplish this. Subsequently, the matrix equation $[Z]\{I\} = \{V\}$, where $[Z]$ represents the impedance matrix, $\{I\}$ denotes the unknown vector, and $\{V\}$ represents the excitation vector, is solved.

Initially, the problem is solved by assuming that the main problem of a perfect electric conductor (PEC) object has an unknown N without utilizing symmetry. Establishing the connection between each element on the structure's surface is necessary to achieve this. Consequently, the electric field integral equation (EFIE) is discretized with the MoM, and the following linear system is obtained [6].

$$\begin{bmatrix} Z_{11} & Z_{12} & \cdots & Z_{1N} \\ Z_{21} & Z_{22} & \cdots & Z_{2N} \\ \vdots & \vdots & \ddots & \vdots \\ Z_{N1} & Z_{N2} & \cdots & Z_{NN} \end{bmatrix} \begin{bmatrix} I_1 \\ I_2 \\ \vdots \\ I_N \end{bmatrix} = \begin{bmatrix} V_1 \\ V_2 \\ \vdots \\ V_N \end{bmatrix} \tag{1}$$

with

$$Z_{pq} = -j\omega\mu_0 \int_{f_p} \mathbf{f}_p(\mathbf{r}) \cdot \left[1 + \frac{1}{k_0^2} \nabla\nabla\cdot \right] \int_{f_q} \mathbf{f}_q(\mathbf{r}') G_0(\mathbf{r}, \mathbf{r}') d\mathbf{r}' d\mathbf{r} \tag{2}$$

$$V_p = -\int_{f_p} \mathbf{f}_p(\mathbf{r}) \cdot \mathbf{E}^i(\mathbf{r}) d\mathbf{r} \tag{3}$$

In these relations, $\mathbf{f}_p$ and $\mathbf{f}_q$ are the basis functions related to observation area f_p and source area f_q, respectively. In addition, $k_0 = 2\pi/\lambda$ is the free space wave number, and $G_0(\mathbf{r}, \mathbf{r}')$ is the free space Green's function, which is defined as follows:

$$G_0(\mathbf{r}, \mathbf{r}') = \frac{e^{-jk_0|\mathbf{r}-\mathbf{r}'|}}{4\pi\,|\mathbf{r}-\mathbf{r}'|} \tag{4}$$

It has been demonstrated that the MoM requires memory and calculation time of the order $O(N^2)$ and $O(N^3)$, respectively, to solve this problem.

Another approach for solving full-wave scattering problems is utilizing the MLFMM method, which boxes the structure and reduces the number of nodes. With this method, the memory requirement for the number of unknowns N decreases from approximately $O(N^2)$ in the MoM to about $O(N \log N)$ in the MLFMM method. However, as mentioned in the introduction, this method has limitations and loses its efficiency when dealing with dielectric structures and solving monostatic scattering.

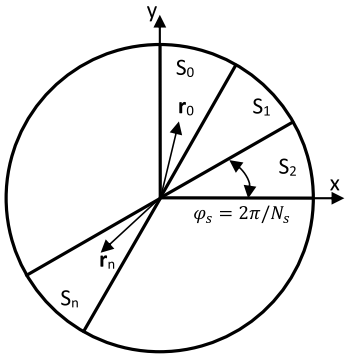

FIGURE 1. Discrete bodies of revolution object with N_s symmetric sectors.

B. SOLVING SCATTERING PROBLEMS USING THE DBOR METHOD

Based on the issues mentioned above, it is necessary to employ efficient methods for analyzing these structures. In structures analyzed using the DBOR method, the memory requirements and computational time decrease by factors of N_s^2 and N_s^3, respectively, where N_s represents the number of discontinuities in the structure. However, as shown in Section V, lower ratios are obtained. The reason for this is the need to use intermediate variables in the program codes related to the DBOR method and the overhead computations that need to be repeated multiple times.

The structure under investigation is shown in Fig. 1. It is a discrete rotating body with N_s symmetric sectors. In order to employ efficient methods for analyzing these structures, it is necessary first to obtain the impedance matrix between each sector and then form the total impedance matrix as follows:

$$[Z] = \begin{bmatrix} Z^{(0)} & Z^{(1)} & \cdots & Z^{(\mathrm{N_s}-1)} \\ Z^{(\mathrm{N_s}-1)} & Z^{(0)} & \cdots & Z^{(\mathrm{N_s}-2)} \\ \vdots & \vdots & \vdots & \vdots \\ Z^{(1)} & Z^{(2)} & \cdots & Z^{(0)} \end{bmatrix} \tag{5}$$

The matrix consists of submatrices, each representing the relationship between different sectors. Specifically, the submatrix $Z^{(0)}$ represents the impedance matrix associated with the source and observation elements in sector zero. Similarly, the submatrix $Z^{(1)}$ corresponds to the impedance matrix of the source and observation elements in sectors zero and one, respectively. Equation (5) demonstrates that this matrix is a block circulant matrix with unique symmetry, resulting in significantly reduced calculations compared to (1).

C. THE METHOD OF SOLVING MATRIX EQUATIONS WITH BLOCK CIRCULANT

The matrix equation of the MoM for a discrete bodies of revolution can be written in the form [23]:

$$\begin{bmatrix} Z^{(0)} & Z^{(1)} & \cdots & Z^{(N_s-1)} \\ Z^{(N_s-1)} & Z^{(0)} & \cdots & Z^{(N_s-2)} \\ \vdots & \vdots & \ddots & \vdots \\ Z^{(1)} & Z^{(2)} & \cdots & Z^{(0)} \end{bmatrix} \begin{bmatrix} \{I\}^{(0)} \\ \{I\}^{(1)} \\ \vdots \\ \{I\}^{(N_s-1)} \end{bmatrix} = \begin{bmatrix} \{V\}^{(0)} \\ \{V\}^{(1)} \\ \vdots \\ \{V\}^{(N_s-1)} \end{bmatrix} \tag{6}$$

Equation (6) describes an impedance matrix that possesses the specifications outlined in (5). When dealing with a matrix equation involving an impedance matrix with a block circulation property, it is possible to employ more straightforward methods for solving the equation than conventional approaches. Most of the time and cost associated with solving matrix equations are typically attributed to the construction and inversion of the impedance matrix.

Considering the matrix equation mentioned above, if we multiply the k^{th} row by the term $\exp(-jmk\varphi_s)$ and subsequently sum all the rows, we obtain the following result [23], [28]:

$$[Z]_m \{I\}_m = \{V\}_m \tag{7}$$

where

$$[Z]_m = \sum_{k=0}^{N_s-1} Z^{(k)} e^{jmk\varphi_s} \tag{8}$$

$$\{I\}_m = \sum_{k=0}^{N_s-1} \{I\}^{(k)} e^{-jmk\varphi_s} \tag{9}$$

$$\{V\}_m = \sum_{k=0}^{N_s-1} \{V\}^{(k)} e^{-jmk\varphi_s} \tag{10}$$

with $\varphi_s = 2\pi/N_s$. Equations (9) and (10) define the Discrete Fourier Transform (DFT), and its inverse is defined as follows:

$$\{I\}^{(k)} = \frac{1}{N_s} \sum_{m=0}^{N_s-1} \{I\}_m e^{jmk\varphi_s} \tag{11}$$

$$\{V\}^{(k)} = \frac{1}{N_s} \sum_{m=0}^{N_s-1} \{V\}_m e^{jmk\varphi_s} \tag{12}$$

The formulation provides an efficient solution for (6). Initially, by knowing the excitation values $\{V\}^{(k)}$ for $k = 0, 1, , N_s - 1$, we can calculate the Fourier modes of $\{V\}_m$ for $m = 0, 1, , N_s - 1$ using (10). Subsequently, by solving (7), we obtain $\{I\}_m$ for $m = 0, 1, , N_s - 1$. With the values of $\{I\}_m$ determined, we can utilize (11) to obtain the response vector $\{I\}^{(k)}$ for $k = 0, 1, , N_s - 1$.

The dimension of (7) is N_s times smaller than the dimension of (6). Consequently, compared to the direct method of solving the matrix equation, the required memory and calculation time decreases with ratios of N_s^2 and N_s^3, respectively.

D. MATRIX EXTRACTION WITH BLOCK CIRCULANT PROPERTY

To demonstrate the derivation of (5) and (6), we refer to Fig. 1. Assuming that each sector contains Q elements and the total number of elements is N, the vector representing the unknown current associated with sector n_s can be expressed as follows [20], [21]:

$$\{I\}^{(n_s)} = \left[I_0^{(n_s)}, I_1^{(n_s)}, \cdots, I_q^{(n_s)}, \cdots, I_{Q-1}^{(n_s)} \right]^T \tag{13}$$

where the unknown current $I_q^{(n_s)}$ corresponds to the q^{th} element of the n_s^{th} sector. Similarly, the m_s^{th} sector of the excitation vector can be expressed as follows:

$$\{V\}^{(m_s)} = \left[V_0^{(m_s)}, V_1^{(m_s)}, \cdots, V_q^{(m_s)}, \cdots, V_{Q-1}^{(m_s)} \right]^T \tag{14}$$

where the excitation $V_q^{(m_s)}$ corresponds to the q^{th} element of the m_s^{th} sector. The sectors n_s and m_s represent a sector where the source point is located and a sector where the observation point is located, respectively. Consequently, the surface current distribution of the structure can be expressed as follows:

$$\mathbf{J}(\mathbf{r}) = \sum_{m=0}^{N_s-1} \sum_{q=1}^{Q} I_q^m \mathbf{f}_q \left(\overline{\overline{R}}^m \mathbf{r_0} \right) \quad ; \quad \mathbf{r_0} \in S_0 \tag{15}$$

Referring to Fig. 1, we relate the vector $\mathbf{r}_n$, whose tail-end is in the n^{th} sector, to the vector $\mathbf{r}_0$, whose tail-end is in the zeroth sector. To achieve this objective,

$$\mathbf{r}_n = \overline{\overline{R}}^n \mathbf{r}_0 \tag{16}$$

$$\overline{\overline{R}}(\varphi_s) = \begin{bmatrix} \cos(\varphi_s) & -\sin(\varphi_s) & 0 \\ \sin(\varphi_s) & \cos(\varphi_s) & 0 \\ 0 & 0 & 1 \end{bmatrix} \tag{17}$$

In these relations, $\overline{\overline{R}}$ is the rotation matrix with the following properties:

$$\overline{\overline{R}}^{-1}(\varphi_s) = \overline{\overline{R}}^T(\varphi_s) \tag{18}$$

$$\overline{\overline{R}}^n(\varphi_s) = \overline{\overline{R}}(n\varphi_s) \tag{19}$$

Hence, if Rao-Wilton-Glisson (RWG) basis functions are used, based on the linear property of these functions [29], we obtain

$$\mathbf{f}_q \left(\overline{\overline{R}}^n \mathbf{r} \right) = \overline{\overline{R}}^n \mathbf{f}_q(\mathbf{r}) \tag{20}$$

According to the obtained properties, the elements of the impedance matrix for the EFIE case can be obtained as follows:

$$Z_{pq}^{(m_s,n_s)} = -j\omega\mu_0 \int_{f_{p0}} \mathbf{f}_p(\mathbf{r}) \overline{\overline{R}}^{-m_s} \cdot \left[1 + \frac{1}{k_0^2} \nabla\nabla\cdot \right] \int_{f_{q0}} \overline{\overline{R}}^{n_s} \mathbf{f}_q(\mathbf{r}') G_0(\overline{\overline{R}}^{m_s} \mathbf{r}, \overline{\overline{R}}^{n_s} \mathbf{r}') d\mathbf{r}' d\mathbf{r} \tag{21}$$

In this equation, $Z_{pq}^{(m_s,n_s)}$ represents an element of the impedance matrix, where the source point is located in the

n_s^{th} sector and the observation point is in the m_s^{th} sector. Additionally, f_{p0} and f_{q0} denote the observation and source areas, respectively, in the zeroth sector. Here, $m_s = 0$ to $N_s - 1$ and $n_s = 0$ to $N_s - 1$. The submatrix corresponding to the interaction between the elements of the m_s^{th} and n_s^{th} sectors can be expressed as follows:

$$[Z]^{(m_s,n_s)} \tag{22}$$

Therefore, (1) can be recast in this form:

$$\begin{bmatrix} Z^{(0,0)} & Z^{(0,1)} & \dots & Z^{(0,N_s-1)} \\ Z^{(1,0)} & Z^{(1,1)} & \dots & Z^{(1,N_s-1)} \\ \vdots & \vdots & \ddots & \vdots \\ Z^{(N_s-1,0)} & Z^{(N_s-1,1)} & \dots & Z^{(N_s-1,N_s-1)} \end{bmatrix} \begin{bmatrix} \{I\}^{(0)} \\ \{I\}^{(1)} \\ \vdots \\ \{I\}^{(N_s-1)} \end{bmatrix} = \begin{bmatrix} \{V\}^{(0)} \\ \{V\}^{(1)} \\ \vdots \\ \{V\}^{(N_s-1)} \end{bmatrix} \tag{23}$$

Now, simplifying (21) yields the following expression:

$$Z_{pq}^{(m_s,n_s)} = -j\omega\mu_0 \int_{f_{p0}} \mathbf{f}_p(\mathbf{r}) \overline{\overline{R}}^{n_s-m_s} \cdot \left[1 + \frac{1}{k_0^2}\nabla\nabla\cdot\right] \int_{f_{q0}} \mathbf{f}_q(\mathbf{r}') G_0(\mathbf{r}, \overline{\overline{R}}^{n_s-m_s}\mathbf{r}') d\mathbf{r}' d\mathbf{r} \tag{24}$$

This relation demonstrates that the matrix $Z_{pq}^{(m_s,n_s)}$ remains unchanged as long as the difference between m_s and n_s is the same [18]. Thus, by introducing $k_s \doteq n_s - m_s$ and considering the periodicity of $\overline{\overline{R}}$ with a period of N_s, we can observe that

$$[Z]^{(k_s)} = [Z]^{(N_s+k_s)} \tag{25}$$

so, for $n_s \geq m_s$

$$[Z]^{(m_s,n_s)} = [Z]^{(k_s)} \tag{26}$$

and for $n_s < m_s$

$$[Z]^{(m_s,n_s)} = [Z]^{(N_s+k_s)} \tag{27}$$

The linear system (6) can be finally obtained from (23) by using properties (26) and (27).

III. APPLYING THE DBOR METHOD TO INTEGRAL EQUATIONS

To apply the DBOR method to the integral equations, we first need to extract the expressions related to these integral equations regularly and then apply the method to them. To illustrate the process of extracting these expressions, we begin with (2). By performing mathematical operations and simplifications, the resulting impedance matrix can be expressed as follows [6]:

$$Z_{pq} = -j\omega\mu_0 \int_{f_p}\int_{f_q} \mathbf{f}_p(\mathbf{r}) \cdot \mathbf{f}_q(\mathbf{r}') G_0(\mathbf{r}, \mathbf{r}') d\mathbf{r}' d\mathbf{r} + \frac{j\omega\mu_0}{k_0^2} \int_{f_p} \nabla \cdot \mathbf{f}_p(\mathbf{r}) \int_{f_q} \nabla' \cdot \mathbf{f}_q(\mathbf{r}') G_0(\mathbf{r}, \mathbf{r}') d\mathbf{r}' d\mathbf{r} \tag{28}$$

For simplicity and to avoid repetition, the expressions $A_v(f_p, f_q)$ and $B_v(f_p, f_q)$ are defined as follows:

$$A_v(f_p, f_q) = j\omega \int_{f_p}\int_{f_q} \mathbf{f}_p(\mathbf{r}) \cdot \mathbf{f}_q(\mathbf{r}') G_v(\mathbf{r}, \mathbf{r}') d\mathbf{r}' d\mathbf{r} \tag{29}$$

$$B_v(f_p, f_q) = j\omega \int_{f_p} \nabla \cdot \mathbf{f}_p(\mathbf{r}) \int_{f_q} \nabla' \cdot \mathbf{f}_q(\mathbf{r}') G_v(\mathbf{r}, \mathbf{r}') d\mathbf{r}' d\mathbf{r} \tag{30}$$

In this relation, v is the index related to the environment, which is considered zero for free space. Therefore, the relationship between the elements of the impedance matrix can be written in the following simplified form:

$$Z_{pq} = \mu_0 \left[-A_0(f_p, f_q) + \frac{1}{k_0^2} B_0(f_p, f_q)\right] \tag{31}$$

Hence, according to the PMCHW formulation, it can be shown that the following relations are used to create the impedance matrix of a dielectric structure or a structure containing dielectric and PEC.

$$Z_{f_p}^{EJ_q} = \sum_v \mu_v \left[-A_v(f_p, f_q) + \frac{1}{k_v^2} B_v(f_p, f_q)\right] \tag{32}$$

$$Z_{f_p}^{EM_q} = \sum_v C_v(f_p, f_q) \tag{33}$$

Also using duality

$$Z_{f_p}^{HJ_q} = -Z_{f_p}^{EM_q} \tag{34}$$

$$Z_{f_p}^{HM_q} = \frac{\epsilon_v}{\mu_v} Z_{f_p}^{EJ_q} \tag{35}$$

In these relations, $Z_{f_p}^{EJ_q}$ represents an element of the impedance matrix where the current related to the source area f_q creates an electric field E on the observation area f_p. There are similar interpretations for the terms $Z_{f_p}^{EM_q}$, $Z_{f_p}^{HJ_q}$, and $Z_{f_p}^{HM_q}$.

Also, according to (33), the expression $C_v(f_p, f_q)$ is as follows:

$$C_v(f_p, f_q) = \frac{1}{4\pi} \int_{f_p} \mathbf{f}_p(\mathbf{r}) \cdot \int_{f_q} \left[(\mathbf{r} - \mathbf{r}') \times \mathbf{f}_q(\mathbf{r}')\right]\left[1 + jk_0 \left|\mathbf{r} - \mathbf{r}'\right|\right] \frac{e^{-jk_0|\mathbf{r}-\mathbf{r}'|}}{|\mathbf{r} - \mathbf{r}'|^3} d\mathbf{r}' d\mathbf{r} \tag{36}$$

Now, if the RWG basis functions are used for $\mathbf{f}_p(r)$ and $\mathbf{f}_q(r')$, the expressions $A_v(f_p, f_q)$, $B_v(f_p, f_q)$ and $C_v(f_p, f_q)$ can be written as follows:

$$A_v(f_p, f_q) = j\omega \frac{l_p l_q}{4A_p^{\pm} A_q^{\pm}} \int_{T_p^{\pm}} \boldsymbol{\rho}_p^{\pm}(\mathbf{r}) \cdot \int_{T_q^{\pm}} \boldsymbol{\rho}_q^{\pm}(\mathbf{r}') G_v^{\pm}(\mathbf{r}, \mathbf{r}') d\mathbf{r}' d\mathbf{r} \tag{37}$$

$$B_v(f_p, f_q) = j\omega \frac{l_p l_q}{A_p^{\pm} A_q^{\pm}} \int_{T_p^{\pm}} \int_{T_q^{\pm}} G_v^{\pm}(\mathbf{r}, \mathbf{r}') d\mathbf{r}' d\mathbf{r} \tag{38}$$

$$C_v(f_p,f_q)=\frac{l_p l_q}{16\pi A_p^{\pm}A_q^{\pm}}\int_{T_p^{\pm}}\boldsymbol{\rho}_p^{\pm}(\mathbf{r})\cdot\int_{T_q^{\pm}}\left[(\mathbf{r}-\mathbf{r}')\times\boldsymbol{\rho}_q^{\pm}(\mathbf{r}')\right]\times\left[1+jk_0\left|\mathbf{r}-\mathbf{r}'\right|\right]\frac{e^{-jk_0|\mathbf{r}-\mathbf{r}'|}}{|\mathbf{r}-\mathbf{r}'|^3}d\mathbf{r}'d\mathbf{r}\tag{39}$$

where $T_p^{\pm}$ and $T_q^{\pm}$ are the RWG triangle pairs corresponding to the observation and source edges, respectively, and located in one sector or two sectors. Additionally, l_p represents the length of the common edge between the RWG triangle pairs $T_p^{\pm}$, A_p signifies the area of the triangle T_p, and $\boldsymbol{\rho}_p^{\pm}(\mathbf{r})$ is a position vector, which is described in [29]. Finally, the DBOR method is applied to the solution of the integral equation by using properties (18) to (20), as follows:

$$\begin{aligned}A_{pq,v}^{(m_s,n_s)}&=j\omega\frac{l_p l_q}{4A_p^{\pm}A_q^{\pm}}\int_{T_{p0}^{\pm}}\int_{T_{q0}^{\pm}}\left[\overline{\overline{R}}^{\,m_s}\boldsymbol{\rho}_p^{\pm}(\mathbf{r})\right]\cdot\left[\overline{\overline{R}}^{\,n_s}\boldsymbol{\rho}_q^{\pm}(\mathbf{r}')\right]\\&\quad\times G_v^{\pm\pm}\left(\overline{\overline{R}}^{\,m_s}\mathbf{r},\overline{\overline{R}}^{\,n_s}\mathbf{r}'\right)d\mathbf{r}'d\mathbf{r}\\&=j\omega\frac{l_p l_q}{4A_p^{\pm}A_q^{\pm}}\int_{T_p^{\pm}}\int_{T_q^{\pm}}\boldsymbol{\rho}_p^{\pm}(\mathbf{r})\cdot\left[\overline{\overline{R}}^{\,k_s}\boldsymbol{\rho}_q^{\pm}(\mathbf{r}')\right]\\&\quad\times G_v^{\pm\pm}\left(\mathbf{r},\overline{\overline{R}}^{\,k_s}\mathbf{r}'\right)d\mathbf{r}'d\mathbf{r}\end{aligned}\tag{40}$$

$$\begin{aligned}B_{pq,v}^{(m_s,n_s)}&=j\omega\frac{l_p l_q}{4A_p^{\pm}A_q^{\pm}}\int_{T_{p0}^{\pm}}\int_{T_{q0}^{\pm}}G_v^{\pm\pm}\left(\overline{\overline{\mathbf{R}}}^{\,m_s}\mathbf{r},\overline{\overline{\mathbf{R}}}^{\,n_s}\mathbf{r}'\right)d\mathbf{r}'d\mathbf{r}\\&=j\omega\frac{l_p l_q}{4A_p^{\pm}A_q^{\pm}}\int_{T_{p0}^{\pm}}\int_{T_{q0}^{\pm}}G_v^{\pm\pm}\left(\mathbf{r},\overline{\overline{\mathbf{R}}}^{\,k_s}\mathbf{r}'\right)d\mathbf{r}'d\mathbf{r}\end{aligned}\tag{41}$$

$$\begin{aligned}C_{mn,v}^{(m_s,n_s)}&=\frac{l_m l_n}{16\pi A_m^{\pm}A_n^{\pm}}\int_{T_{m0}^{\pm}}\int_{T_{n0}^{\pm}}\left[\overline{\overline{R}}^{\,m_s}\boldsymbol{\rho}_m^{\pm}(\mathbf{r})\right]\\&\quad\cdot\left[\left(\overline{\overline{R}}^{\,m_s}\mathbf{r}-\overline{\overline{R}}^{\,n_s}\mathbf{r}'\right)\times\left(\overline{\overline{R}}^{\,m_s}\boldsymbol{\rho}_n^{\pm}(\mathbf{r}')\right)\right]\\&\quad\times\left[1+jk_0\left|\overline{\overline{R}}^{\,m_s}\mathbf{r}-\overline{\overline{R}}^{\,n_s}\mathbf{r}'\right|\right]\frac{e^{-jk_0\left|\overline{\overline{R}}^{\,m_s}\mathbf{r}-\overline{\overline{R}}^{\,n_s}\mathbf{r}'\right|}}{\left|\overline{\overline{R}}^{\,m_s}\mathbf{r}-\overline{\overline{R}}^{\,n_s}\mathbf{r}'\right|^3}d\mathbf{r}'d\mathbf{r}\\&=\frac{l_m l_n}{16\pi A_m^{\pm}A_n^{\pm}}\int_{T_{m0}^{\pm}}\int_{T_{n0}^{\pm}}\boldsymbol{\rho}_m^{\pm}(\mathbf{r})\cdot\left[\left(\mathbf{r}-\overline{\overline{R}}^{\,k_s}\mathbf{r}'\right)\right.\\&\quad\left.\times\boldsymbol{\rho}_n^{\pm}(\mathbf{r}')\right]\left[1+jk_0\left|\mathbf{r}-\overline{\overline{R}}^{\,k_s}\mathbf{r}'\right|\right]\frac{e^{-jk_0\left|\mathbf{r}-\overline{\overline{R}}^{\,k_s}\mathbf{r}'\right|}}{\left|\mathbf{r}-\overline{\overline{R}}^{\,k_s}\mathbf{r}'\right|^3}d\mathbf{r}'d\mathbf{r}\end{aligned}\tag{42}$$

IV. COMBINING THE DBOR AND DDM METHODS

Because few microstrip arrays have discrete rotational symmetry and most of them do not have this symmetry, the applicability of the DBOR method needs to be expanded. The analysis of such structures can be divided into two parts using the DDM to address this. The microstrip lines and their associated patches occupy a significantly smaller area in these structures than the dielectric substrate and ground plane. Consequently, the traditional MoM can be employed to analyze the microstrip lines and patches, while the DBOR method is utilized to analyze the ground plane and dielectric

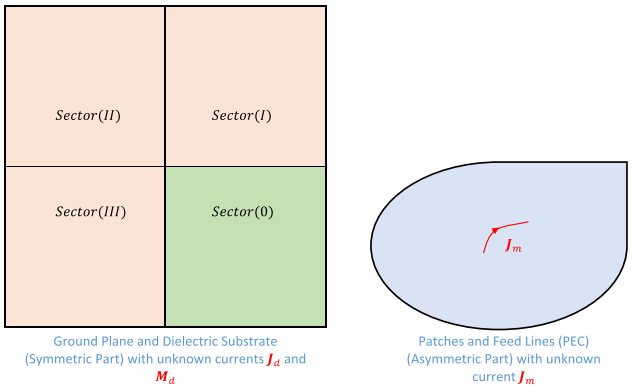

FIGURE 2. Schematic representation of the use of DDM in the separation of symmetric and asymmetric parts of a microstrip antenna.

substrate. Combining these two methods using the DDM technique can obtain the desired solution. As depicted in Fig. 2, we can apply the DDM technique to investigate the problem of a microstrip array. The figure illustrates two distinct structures. The structure on the left comprises the ground and substrate, and only one sector is analyzed using the DBOR method due to its symmetry. On the other hand, the structure on the right pertains to patches and feed lines, which is analyzed using the traditional MoM.

Based on Fig. 2, we assume that the unknown currents in the symmetrical part are $\mathbf{J}_d$ and $\mathbf{M}_d$, while the unknown current in the asymmetrical part is $\mathbf{J}_m$. To solve this problem using the traditional MoM, the following matrix equation is formed:

$$\begin{bmatrix}Z_d^{EJ_d} & Z_d^{EM_d} & Z_d^{EJ_m}\\ Z_d^{HJ_d} & Z_d^{HM_d} & Z_d^{HJ_m}\\ Z_m^{EJ_d} & Z_m^{EM_d} & Z_m^{EJ_m}\end{bmatrix}\begin{bmatrix}\mathbf{J}_d\\ \mathbf{M}_d\\ \mathbf{J}_m\end{bmatrix}=\begin{bmatrix}\mathbf{V}_d^E\\ \mathbf{V}_d^H\\ \mathbf{V}_m^E\end{bmatrix}\tag{43}$$

where $\mathbf{V}_{f_p}^{E/H}$ is a component of the excitation vector that shows the effect of Electric/Magnetic field incident on the f_p area. The unknown currents in both parts are determined upon solving this matrix equation. However, to address this problem using a combination of the traditional MoM and DBOR, the following equations can be derived from (43) for symmetric and asymmetric parts.

$$Z_{dd}\{I_d\}+Z_{dm}\mathbf{J}_m=\{V_d\}\tag{44}$$

$$Z_{md}\{I_d\}+Z_m^{EJ_m}\mathbf{J}_m=\mathbf{V}_m^E\tag{45}$$

where

$$Z_{dd}=\begin{bmatrix}Z_d^{EJ_d} & Z_d^{EM_d}\\ Z_d^{HJ_d} & Z_d^{HM_d}\end{bmatrix}\tag{46}$$

$$Z_{dm}=\begin{bmatrix}Z_d^{EJ_m} & Z_d^{HJ_m}\end{bmatrix}^T\tag{47}$$

$$Z_{md}=\begin{bmatrix}Z_m^{EJ_d} & Z_m^{EM_d}\end{bmatrix}\tag{48}$$

$$\{I_d\} = \left[\mathbf{J}_d \ \mathbf{M}_d\right]^T \tag{49}$$

$$\{V_d\} = \left[\mathbf{V}_d^E \ \mathbf{V}_d^H\right]^T \tag{50}$$

Based on (44) and (45), it is evident that the symmetric and asymmetric parts of the structure are coupled to each other. Consequently, to address this issue, we derive the unknown current $\{I_d\}$ from (44) and incorporate it in (45) as follows:

$$\{I_d\} = Z_{dd}^{-1}\{V_d\} - Z_{dd}^{-1}Z_{dm}\mathbf{J}_m \tag{51}$$

$$\mathbf{J}_m = \left[Z_m^{EJ_m} - Z_{md}Z_{dd}^{-1}Z_{dm}\right]^{-1}\left\{\mathbf{V}_m^E - Z_{md}Z_{dd}^{-1}\{V_d\}\right\} \tag{52}$$

While (52) can be readily solved through traditional matrix equation-solving techniques; we opt to utilize the DBOR method to leverage the symmetry property associated with the symmetric part. As such, certain parts of this equation are solved using the DBOR method. Consequently, we consider the following intermediate equations:

$$\{J_d\} = Z_{dd}^{-1}\{V_d\} \tag{53}$$

$$A = Z_{dd}^{-1}Z_{dm} \tag{54}$$

Given that Z_{dd} is a block circulant matrix, (53) and (54) can be solved by section II-C using the DBOR method. To facilitate this, we restructure these equations as follows:

$$Z_{dd}\{J_d\} = \{V_d\} \tag{55}$$

$$Z_{dd}A = Z_{dm} \tag{56}$$

By employing the DBOR method to solve (55) and (56) and subsequently determining $\{J_d\}$ and A, we can derive the response associated with the unknown current in the asymmetric part using (52). On the other hand, by determining $\mathbf{J}_m$, the unknown current in the symmetrical part is obtained by (51), and the problem is completely solved.

Notably, in (56), A and Z_{dm} are matrices. Therefore, to effectively solve this equation, we must consider the matrix Z_{dd} in conjunction with the columns of A and Z_{dm}. For instance, let's assume that the matrices A and Z_{dm} take the following form:

$$A = \left[\{a_0\}, \{a_1\}, \cdots, \{a_i\}, \cdots, \{a_{M-1}\}\right] \tag{57}$$

$$Z_{dm} = \left[\{z_0\}, \{z_1\}, \cdots, \{z_i\}, \cdots, \{z_{M-1}\}\right] \tag{58}$$

where $\{a_i\}$ and $\{z_i\}$ represent the vectors of the i^{th} column of matrices A and Z_{dm}, respectively; also, M represents the number of unknowns in the asymmetric part. Consequently, to effectively solve (56), it becomes necessary to solve the following M equations utilizing the DBOR method.

$$Z_{dd}\{a_i\} = \{z_i\}; \quad i = 0, 1, \cdots, M-1 \tag{59}$$

The approach to solving each of these equations is similar to that of solving (55). However, since the coefficients matrix Z_{dd} remains consistent across all these equations, the computational effort required for solving (56) exceeds that of (55) solely in M operations for matrix multiplication, DFT, and Inverse DFT (IDFT). Consequently, the problem is resolved with remarkable speed.

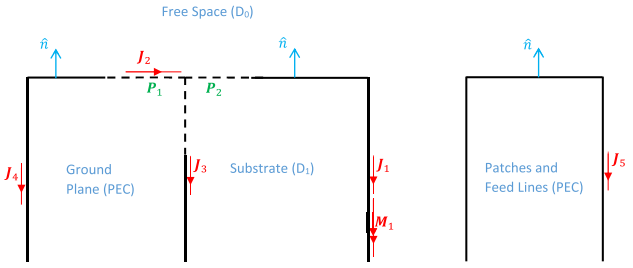

FIGURE 3. Implementation of the DDM for scattering analysis of a microstrip array.

As evident from (52), it comprises two distinct sentences. The first sentence solely incorporates the impedance matrix of both symmetric and asymmetric parts and their interaction impedance matrix. In contrast, the subsequent sentence relies on the excitation vectors $\mathbf{V}_m^E$ and $\{V_d\}$. Consequently, the first sentence exclusively depends on the structure and remains invariant across all radiation and scattering angles. Furthermore, given the larger area of the symmetric part compared to the asymmetric part, applying the proposed method significantly reduces the computation time and memory requirements for problem-solving relative to the traditional MoM. A notable advantage of this method over iterative methods is the simultaneous and direct solution of (44) and (45), thereby substantially accelerating the problem-solving process.

To form the matrix equation of the original problem that includes both symmetric and asymmetric parts and apply the traditional MoM to it; we consider Fig. 3. The electric and magnetic surface currents depicted in the figure are defined as follows:

$$\mathbf{J}_1 = \sum_{n=1}^{N_1} a_n\mathbf{f}_n(\mathbf{r}) \quad ; \quad \mathbf{M}_1 = \sum_{n=1}^{N_1} b_n\mathbf{f}_n(\mathbf{r}) \tag{60}$$

$$\mathbf{J}_2 = \underbrace{\sum_{n=1}^{N_2} c_n\mathbf{f}_n(\mathbf{r})}_{\text{current (I)}} = \underbrace{\sum_{n=1}^{N_2} c_n\left(\mathbf{P}_1 + \mathbf{P}_2\right)(\mathbf{r})}_{\text{current (II)}} \tag{61}$$

$$\mathbf{J}_3 = \sum_{n=1}^{N_3} d_n\mathbf{f}_n(\mathbf{r}) \ ; \ \mathbf{J}_4 = \sum_{n=1}^{N_4} e_n\mathbf{f}_n(\mathbf{r}) \ ; \ \mathbf{J}_5 = \sum_{n=1}^{N_5} h_n\mathbf{f}_n(\mathbf{r}) \tag{62}$$

In these equations, $\mathbf{f}_n$ represents the RWG-type basis function, while $\mathbf{P}_1$ and $\mathbf{P}_2$ denote the half-triangles of the RWG basis function. By combining the half-triangles forms a pair of RWG triangles. Additionally, N_i specifies the number of triangle pairs in surfaces with index $i = 1$ to 5. In (61), the current (I) corresponds to the surface current $\mathbf{J}_2$ in the D_1 region, while the current (II) corresponds to the surface current $\mathbf{J}_2$ in the D_0 region. Thus, the corresponding matrix

equation is as follows:

$$\begin{bmatrix} Z_{f_1}^{EJ_1} & Z_{f_1}^{EM_1} & Z_{f_1}^{EJ_2} & Z_{f_1}^{EJ_3} & Z_{f_1}^{EJ_4} & Z_{f_1}^{EJ_5} \\ Z_{f_1}^{HJ_1} & Z_{f_1}^{HM_1} & Z_{f_1}^{HJ_2} & Z_{f_1}^{HJ_3} & Z_{f_1}^{HJ_4} & Z_{f_1}^{HJ_5} \\ Z_{f_2}^{EJ_1} & Z_{f_2}^{EM_1} & Z_{f_2}^{EJ_2} & Z_{f_2}^{EJ_3} & Z_{f_2}^{EJ_4} & Z_{f_2}^{EJ_5} \\ Z_{f_3}^{EJ_1} & Z_{f_3}^{EM_1} & Z_{f_3}^{EJ_2} & Z_{f_3}^{EJ_3} & [0] & [0] \\ Z_{f_4}^{EJ_1} & Z_{f_4}^{EM_1} & Z_{f_4}^{EJ_2} & [0] & Z_{f_4}^{EJ_4} & Z_{f_4}^{EJ_5} \\ Z_{f_5}^{EJ_1} & Z_{f_5}^{EM_1} & Z_{f_5}^{EJ_2} & [0] & Z_{f_5}^{EJ_4} & Z_{f_5}^{EJ_5} \end{bmatrix} \begin{bmatrix} \mathbf{J}_1 \\ \mathbf{M}_1 \\ \mathbf{J}_2 \\ \mathbf{J}_3 \\ \mathbf{J}_4 \\ \mathbf{J}_5 \end{bmatrix} = \begin{bmatrix} \mathbf{V}_1^E \\ \mathbf{V}_1^H \\ \mathbf{V}_2^E \\ \mathbf{0} \\ \mathbf{V}_4^E \\ \mathbf{V}_5^E \end{bmatrix} \tag{63}$$

Referring to Fig. 3 and (63), the combined method has divided the problem-solving process into two parts. One part is related to patches and feeding lines, while the other is related to the ground and the dielectric substrate.

Equation (63), derived through the application of the traditional MoM, can be solved using standard matrix equation-solving techniques, yielding solutions that represent surface currents. However, to employ the DDM in addressing this problem, (63) can be viewed as corresponding to (43) and solved accordingly. As a result, we modify (44) and (45) to suit this problem as follows:

$$Z_{dd}\{I_d\} + Z_{dm}\mathbf{J}_5 = \{V_d\} \tag{64}$$

$$Z_{md}\{I_d\} + Z_{f_5}^{EJ_5}\mathbf{J}_5 = \mathbf{V}_5^E \tag{65}$$

where

$$Z_{dd} = \begin{bmatrix} Z_{f_1}^{EJ_1} & Z_{f_1}^{EM_1} & Z_{f_1}^{EJ_2} & Z_{f_1}^{EJ_3} & Z_{f_1}^{EJ_4} \\ Z_{f_1}^{HJ_1} & Z_{f_1}^{HM_1} & Z_{f_1}^{HJ_2} & Z_{f_1}^{HJ_3} & Z_{f_1}^{HJ_4} \\ Z_{f_2}^{EJ_1} & Z_{f_2}^{EM_1} & Z_{f_2}^{EJ_2} & Z_{f_2}^{EJ_3} & Z_{f_2}^{EJ_4} \\ Z_{f_3}^{EJ_1} & Z_{f_3}^{EM_1} & Z_{f_3}^{EJ_2} & Z_{f_3}^{EJ_3} & [0] \\ Z_{f_4}^{EJ_1} & Z_{f_4}^{EM_1} & Z_{f_4}^{EJ_2} & [0] & Z_{f_4}^{EJ_4} \end{bmatrix} \tag{66}$$

$$Z_{dm} = \left[Z_{f_1}^{EJ_5}, Z_{f_1}^{HJ_5}, Z_{f_2}^{EJ_5}, [0], Z_{f_4}^{EJ_5}\right]^T \tag{67}$$

$$Z_{md} = \left[Z_{f_5}^{EJ_1}, Z_{f_5}^{EM_1}, Z_{f_5}^{EJ_2}, [0], Z_{f_5}^{EJ_4}\right] \tag{68}$$

$$\{I_d\} = [\mathbf{J}_1, \mathbf{M}_1, \mathbf{J}_2, \mathbf{J}_3, \mathbf{J}_4]^T \tag{69}$$

$$\{V_d\} = \left[\mathbf{V}_1^E, \mathbf{V}_1^H, \mathbf{V}_2^E, \mathbf{0}, \mathbf{V}_4^E\right]^T \tag{70}$$

Now, we can consider (64) and (65) as corresponding to (44) and (45), and solve them as we did previously. Therefore, we modify (51) and (52) according to this problem as follows:

$$\{I_d\} = Z_{dd}^{-1}\{V_d\} - Z_{dd}^{-1}Z_{dm}\mathbf{J}_5 \tag{71}$$

$$\mathbf{J}_5 = \left[Z_{f_5}^{EJ_5} - Z_{md}Z_{dd}^{-1}Z_{dm}\right]^{-1}\left\{\mathbf{V}_5^E - Z_{md}Z_{dd}^{-1}\{V_d\}\right\} \tag{72}$$

By solving these equations like before, we obtain the unknown currents in both the symmetrical and asymmetrical parts, thereby completely solving the problem.

V. SIMULATION RESULTS

In the previous sections, we explained how to analyze the scattering from objects with discrete axial symmetry using the DBOR and DDM methods. In this section, we explore specific examples of microstrip arrays with discrete axial symmetry characteristics. To validate the precision and accuracy of the results obtained through our proposed method, we compare them with those obtained from the numerical method of FEKO software.

Additionally, we compare the DBOR and the combined DBOR+DDM methods with a traditional MoM to assess their speed and memory requirements for analyzing a microstrip array. Throughout this comparison, we keep the effective parameters consistent, including the programmer, software, programming language, hardware used, and the manner and mesh size of the structure. Therefore, the DBOR and the combined DBOR+DDM methods only affect the calculation time and the required memory.

In the following sections, firstly, we examine the asymptotic method for analyzing wave scattering from microstrip arrays. This study highlights the limitations of the asymptotic method when analyzing structures that include dielectric materials.

Finally, we investigate wave scattering from various antennas and microstrip absorbers.

A. ASYMPTOTIC METHODS IN SCATTERING ANALYSIS OF MICROSTRIP ARRAYS

Asymptotic and numerical methods are employed to calculate the scattered field of a structure. Asymptotic methods are widely used under the following conditions [1], [2], [3], [4], [5], [6]:

- Objects with dimensions larger than the wavelength.
- PEC objects.
- The main lobe of the scattering field.

To investigate this matter, we analyze the array antenna depicted in Fig. 4 using the asymptotic and the MoM methods available in the CST commercial software. However, it should be noted that the asymptotic method in the CST software cannot analyze lossy dielectrics. Consequently, it becomes necessary to analyze the scattered field of the array antenna shown in Fig. 4 for two scenarios. One with a lossy substrate and the other with a loss-free substrate, using the MoM. The dielectric material employed in the substrate possesses a loss tangent of 0.025. By subjecting this antenna to analysis using both the asymptotic and moment methods, we obtain the graphs presented in Figs. 5 and 6. As depicted in the figures, the scattering field obtained through the asymptotic method differs from the result obtained through the MoM for all angles to be examined. Consequently, it is not appropriate

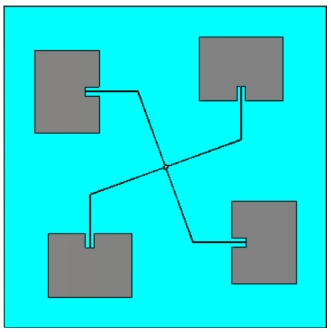

FIGURE 4. A square microstrip array antenna with 140mm length, 2.4mm height, 36.19mm patch length, 27.88mm patch width, FR4 dielectric substrate with $\epsilon_r = 4.7$ and loss tangent of 0.025.

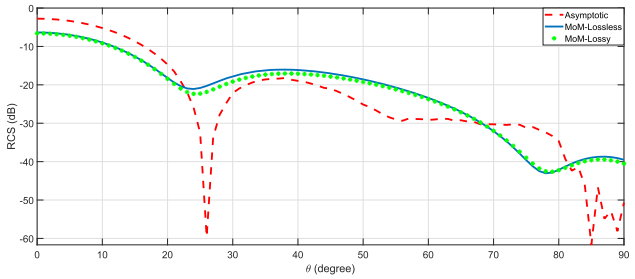

FIGURE 5. Comparison of the scattered fields from square array antenna at 2.4GHz frequency, using the MoM and asymptotic methods for V-Pole by the CST commercial software.

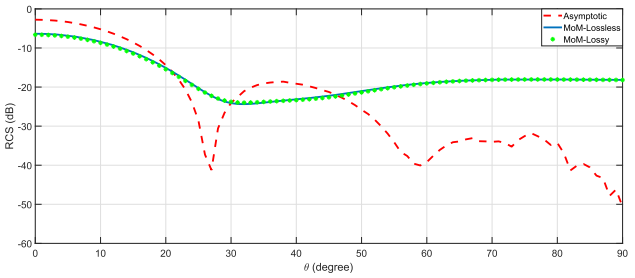

FIGURE 6. Comparison of the scattered fields from square array antenna at 2.4GHz frequency, using the MoM and asymptotic methods for H-Pole by the CST commercial software.

to use asymptotic methods in structures containing dielectric whose thickness is comparable to wave penetration depth.

B. THE DBOR METHOD IN SCATTERING ANALYSIS OF MICROSTRIP ARRAYS

This section considers three examples to demonstrate the effectiveness of the DBOR method in analyzing the scattering of structures with DBOR symmetry. In all the following examples, an FR4 dielectric substrate with $\epsilon_r = 4.7$ and a loss tangent of 0.025 is utilized. Also, we utilize three colors for each structure's parts. Blue, green, and red represent the ground plane, substrate, and patches, respectively.

For the first example, we consider a quarter of the microstrip antenna, as shown in Fig. 7. These antennas are widely used to produce circularly polarized electromagnetic

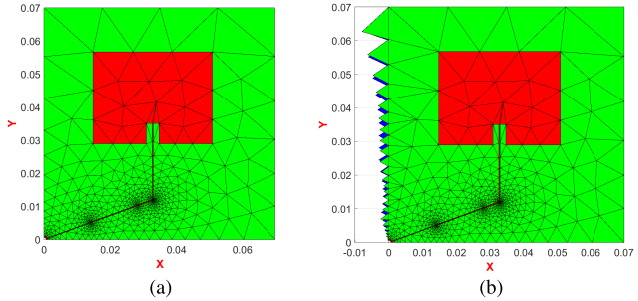

FIGURE 7. A quarter of the meshed square microstrip array antenna with 70mm length, 2.4mm thickness, 36.19mm patch length, 27.88mm patch width, FR4 dielectric substrate with $\epsilon_r = 4.7$ and loss tangent of 0.025. (a) without continuity of boundary meshes. (b) with the continuity of the boundary meshes.

waves [30]. Based on the figure, the antenna under consideration exhibits DBOR symmetry, making it suitable for analysis using the DBOR method. The complete antenna has dimensions of 140mm in length and width, with a substrate thickness of 2.4mm.

Since the basis functions used in solving this problem are of the RWG type, the unknown currents are assigned to the common edges of triangle pairs. Therefore, it is necessary to consider all the edges shared between two triangles in the complete structure of the microstrip array to form a triangle pair as common edges in the DBOR method and include them in the calculations. However, as shown in Fig. 7a, the edges located on the y-axes are considered as the boundary edges of the triangles and are not included in the calculations. It is necessary to rotate the boundary triangles located on the x-axes by an angle of 90 degrees counterclockwise and place them on the y-axes [15] to compensate for this deficiency. By doing this and some modifications, the boundary triangles on the y-axes are treated as triangle pairs, and their edges are considered as common edges of a triangle pair and included in the calculations. This process is illustrated in Fig. 7b. So, the microstrip array shown in Fig. 7b can be analyzed using the DBOR method to determine the scattered fields.

To analyze this antenna, we first obtain its scattered field using the DBOR method and then compare it with the results obtained from FEKO software and the traditional MoM regarding accuracy, speed, and required memory, respectively. The Radar Cross Section (RCS) of this antenna at a frequency of 2.4GHz, in the $\phi = 0$ plane for V and H polarizations, are shown in Figs. 8 and 9, respectively.

For the second example, we consider a quarter of the FSS absorber depicted in Fig. 10. This absorber also possesses DBOR symmetry, enabling the DBOR method for analysis. The complete FSS has dimensions of 72mm in length and width, with a substrate thickness of 0.75mm [31]. The RCS of this absorber at a frequency of 10.85GHz, in the $\phi = 0$ plane for V and H polarizations are shown in Figs. 11 and 12, respectively.

As a third example, we examine a cylindrical microstrip antenna array with seven symmetrical sectors, as depicted

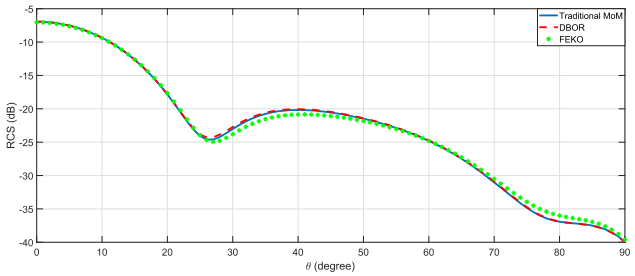

FIGURE 8. Comparison of the scattered field related to the DBOR microstrip antenna array at the frequency of 2.4GHz and in $\phi = 0$ plane with V-Pole for the traditional MoM (Full Structure), the DBOR method, and the obtained results from the commercial FEKO software.

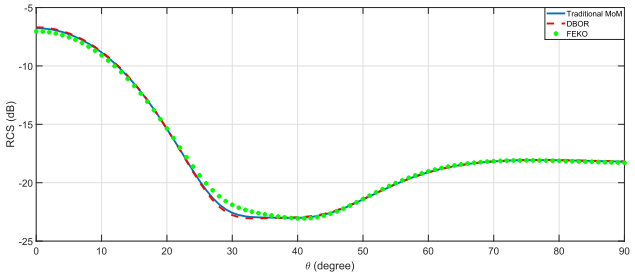

FIGURE 9. Comparison of the scattered field related to the DBOR microstrip antenna array at the frequency of 2.4GHz and in $\phi = 0$ plane with H-Pole for thr traditional MoM (Full Structure), the DBOR method, and the obtained results from the commercial FEKO software.

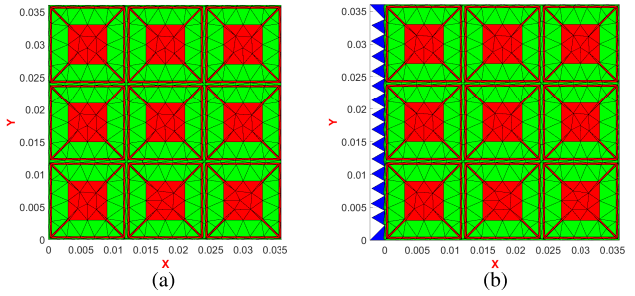

FIGURE 10. A quarter of the meshed square FSS microstrip array with 36mm length, 0.75mm thickness, 5.6mm patch length, FR4 dielectric substrate with $\epsilon_r = 4.7$ and loss tangent of 0.025. (a) without continuity of boundary meshes. (b) with the continuity of the boundary meshes.

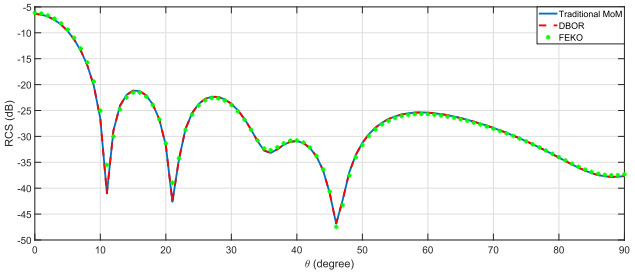

FIGURE 11. Comparison of the scattered field related to the DBOR microstrip FSS array at the frequency of 10.85GHz and in $\phi = 0$ plane with V-Pole for traditional MoM (Full Structure), the DBOR method, and the obtained results from the commercial FEKO software.

in Fig. 13. These antennas are flexible and have various applications, especially in phased array radars [32], [33]. The

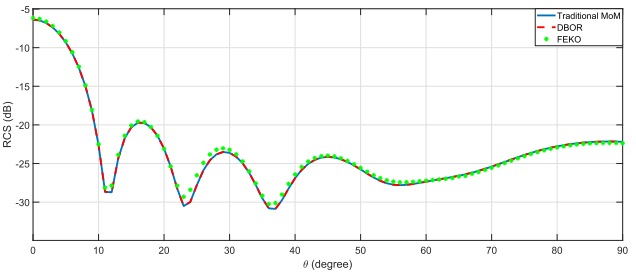

FIGURE 12. Comparison of the scattered field related to the DBOR microstrip FSS array at the frequency of 10.85GHz and in $\phi = 0$ plane with H-Pole for traditional MoM (Full Structure), the DBOR method, and the obtained results from the commercial FEKO software.

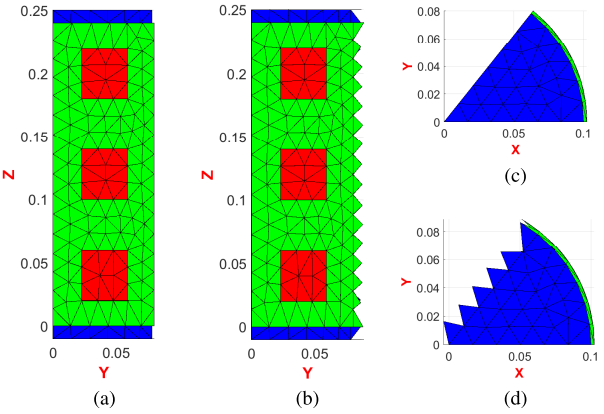

FIGURE 13. A seventh of the meshed cylindrical microstrip array antenna with 240mm height, 2.4mm thickness, 100mm radius, 40mm patch length, FR4 dielectric substrate with $\epsilon_r = 4.7$ and loss tangent of 0.025. (a) and (c) without continuity of boundary meshes. (b) and (d) with the continuity of the boundary meshes.

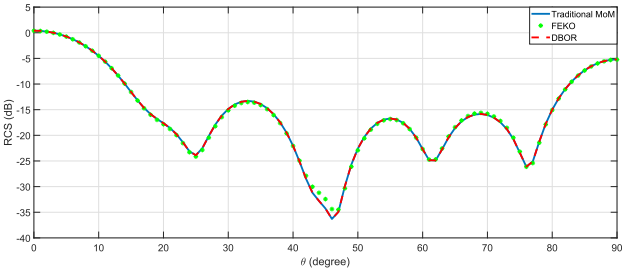

FIGURE 14. Comparison of the scattered field related to the cylindrical microstrip array at the frequency of 2.4GHz and in $\phi = 0$ plane with V-Pole for traditional MoM (Full Structure), the DBOR method, and the obtained results from the commercial FEKO software.

complete antenna has a height of 240mm, a radius of 100mm, and a substrate thickness of 2.4mm.

The RCS of this antenna at a frequency of 2.4GHz, in the $\phi = 0$ plane for V and H polarizations, are shown in Figs. 14 and 15, respectively.

These figures show that the scattered field obtained using the DBOR method has excellent agreement with the results obtained from the traditional MoM and the FEKO software moment method.

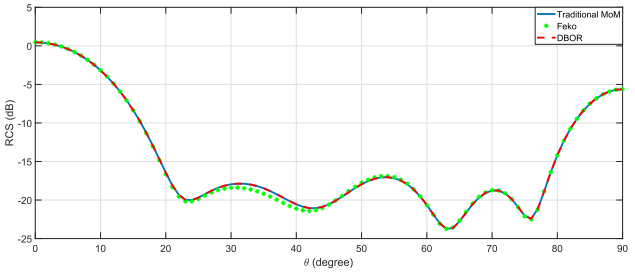

FIGURE 15. Comparison of the scattered field related to the cylindrical microstrip array at the frequency of 2.4GHz and in $\phi = 0$ plane with H-Pole for traditional MoM (Full Structure), the DBOR method, and the obtained results from the commercial FEKO software.

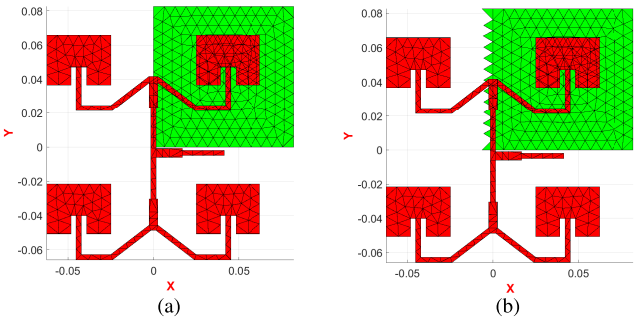

FIGURE 16. A quarter of the meshed square microstrip array antenna with 80mm length, 1.575mm thickness, 37.5mm patch length, 29.06mm patch width, FR4 dielectric substrate with $\epsilon_r = 4.7$ and loss tangent of 0.025. (a) without continuity of boundary meshes. (b) with the continuity of the boundary meshes.

To assess and compare the speed and memory requirements of the proposed method against the traditional MoM, the calculation time and necessary memory for each of these two methods are provided in Table 1 for all the examples. According to the table, the proposed method significantly improves required memory and calculation speed compared to the traditional MoM.

As mentioned in the previous sections, in theory, the reduction in memory requirements and calculation time of the DBOR method compared to the traditional MoM is proportional to N_s^2 and N_s^3, respectively. However, these ratios may not be achieved due to the need to use interface variables in the program codes related to the DBOR method, creating matrix Z_m, and the overhead calculations that need to be repeated several times.

C. THE DBOR+DDM METHOD IN WAVE SCATTERING ANALYSIS OF MICROSTRIP ARRAYS

To assess the effectiveness of the combined DBOR+DDM method for analyzing scattering in composite structures, we investigate a specific case where one section of the structure exhibits discrete symmetry while the other does not. This section presents two examples for analysis. We utilize an FR4 dielectric substrate with $\epsilon_r = 4.7$ and a loss tangent of 0.025 in each example. As before, we utilize the three colors for each structure's parts.

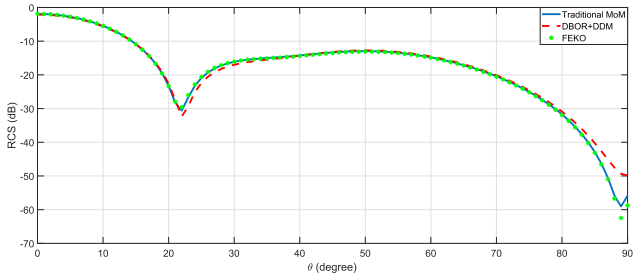

FIGURE 17. Comparison of the scattered field related to the non-DBOR microstrip antenna array at the frequency of 2.4GHz and in $\phi = 0$ plane with V-Pole for traditional MoM (Full Structure), the DBOR method, and the obtained results from the commercial FEKO software.

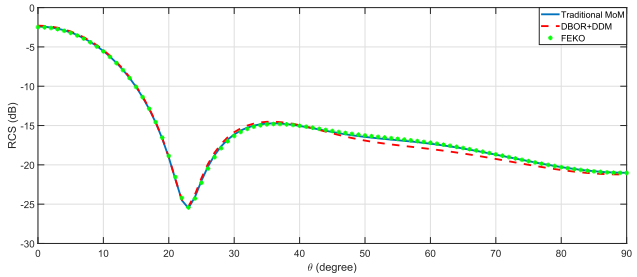

FIGURE 18. Comparison of the scattered field related to the non-DBOR microstrip antenna array at the frequency of 2.4GHz and in $\phi = 0$ plane with H-Pole for traditional MoM (Full Structure), the DBOR method, and the obtained results from the commercial FEKO software.

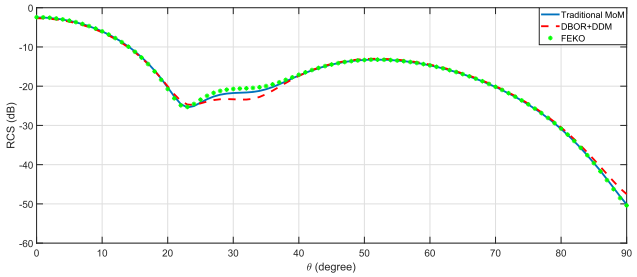

FIGURE 19. Comparison of the scattered field related to the non-DBOR microstrip antenna array at the frequency of 2.4GHz and in $\phi = 90°$ plane with V-Pole for traditional MoM (Full Structure), the DBOR method, and the obtained results from the commercial FEKO software.

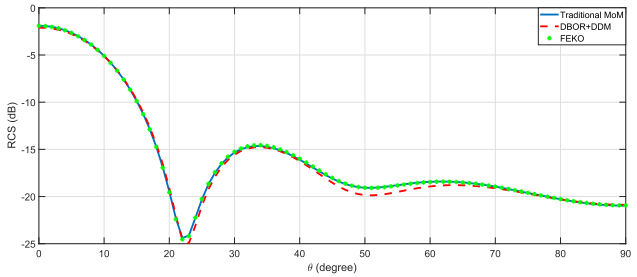

FIGURE 20. Comparison of the scattered field related to the non-DBOR microstrip antenna array at the frequency of 2.4GHz and in $\phi = 90°$ plane with H-Pole for traditional MoM (Full Structure), the DBOR method, and the obtained results from the commercial FEKO software.

To analyze these examples, we first employ the combined DBOR+DDM method to obtain the scattered field. We then

TABLE 1. A comparison of calculation time and memory requirements for the traditional mom and the DBOR method.

Structure	Num. of Unknowns			Required Memory (GB)			Calc. Time(min)		
	Traditional MoM	DBOR	Reduction factor	Traditional MoM	DBOR	Reduction factor (unitless)	Traditional MoM	DBOR	Reduction factor (unitless)
Planar Antenna Array	14803	4001	3.7	14.38	2.29	6.28	313.23	79.29	3.95
Cylindrical Antenna Array	13628	1726	7.9	9.61	0.702	13.69	190.52	21.49	8.87
Planar FSS Absorber	13910	3586	3.88	12.59	1.9	6.63	267.58	64.59	4.14

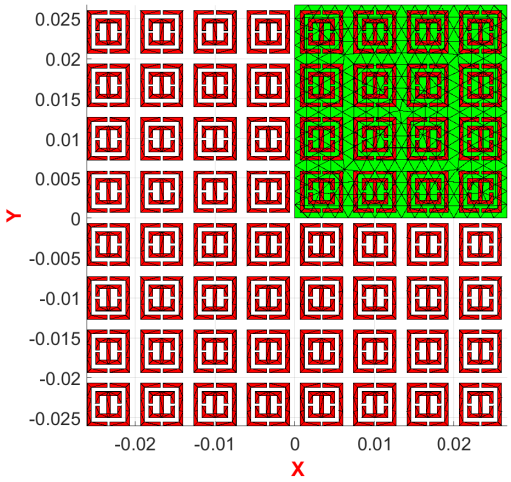

(a) Without continuity of the boundary meshes

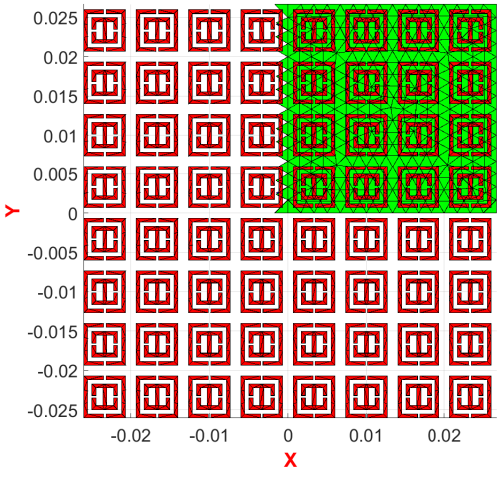

(b) With continuity of the boundary meshes

FIGURE 21. The meshed square FSS microstrip array with 50mm length, 0.75mm thickness, 6.67mm patch length, FR4 dielectric substrate with $\epsilon_r = 4.7$ and loss tangent of 0.025.

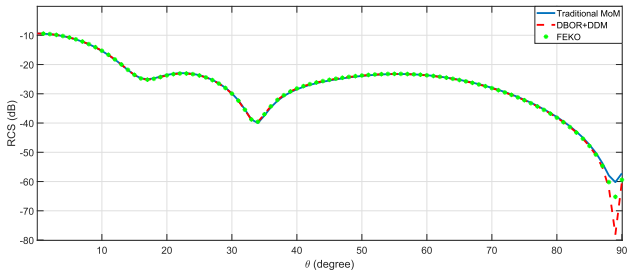

FIGURE 22. Comparison of the scattered field related to the non-DBOR microstrip FSS array at the frequency of 9.85GHz and in $\phi = 0$ plane with V-Pole for traditional MoM (Full Structure), the DBOR method, and the obtained results from the commercial FEKO software.

compare these results with those obtained from FEKO software and the traditional MoM regarding accuracy, speed, and required memory.

As a first example, we focus on a microstrip antenna depicted in Fig. 16. The patches and feeding lines lack discrete rotational symmetry, while the dielectric substrate and ground plane possess such properties. Consequently, we analyze the patches and feeding lines using the traditional MoM, and the dielectric substrate and ground plane using the DBOR method. Finally, we combine both results using the DDM technique. This linearly polarized antenna operates at a central frequency of 2.4 GHz, with dimensions of 160mm in length and width, and 1.6mm in thickness. The RCS of this antenna at a frequency of 2.4GHz, in the $\phi = 0$ and $\phi = 90$ planes for V and H polarizations, are shown in Figs. 17 to 20.

For the second example, we consider an asymmetric FSS absorber as depicted in Fig. 21. The absorber lacks DBOR symmetry, making it suitable for analysis using the combined DBOR+DDM method. The absorber has dimensions of 50mm in length and width, with a substrate thickness of 0.75mm [34]. The RCS of this absorber at a frequency of 9.85GHz, in the $\phi = 0$ and $\phi = 90$ planes for V and H polarizations, are shown in Figs. 22 to 25.

The results obtained by the DBOR+DDM method are consistent with those obtained by both the traditional MoM and the FEKO software MoM, as evident in the figures. Additionally, we compare the speed and required memory of the proposed method with the traditional MoM. Table 2 presents the calculation time and required memory for both methods across all examples. The table demonstrates that the proposed method significantly improves the required

TABLE 2. A comparison of calculation time and memory requirements for the traditional mom and the DBOR+DDM method.

Structure	Num. of Unknowns			Required Memory (GB)			Calc. Time(min)		
	Traditional MoM	DBOR+ DDM	Reduction factor	Traditional MoM	DBOR+ DDM	Reduction factor (unitless)	Traditional MoM	DBOR+ DDM	Reduction factor (unitless)
Planar Antenna Array	13592	3860	3.52	11.66	2.25	5.18	230.32	73.83	3.12
Planar FSS Absorber	16213	5904	2.75	13.65	3.32	4.11	222.34	87.18	2.55

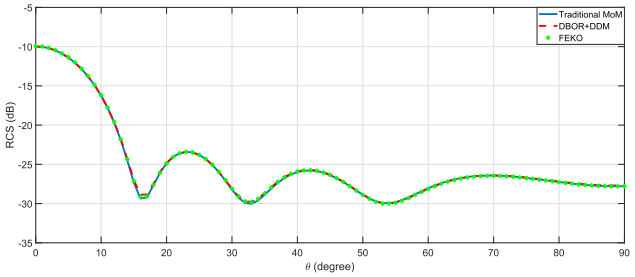

FIGURE 23. Comparison of the scattered field related to the non-DBOR microstrip FSS array at the frequency of 9.85GHz and in $\phi = 0$ plane with H-Pole for traditional MoM (Full Structure), the DBOR method, and the obtained results from the commercial FEKO software.

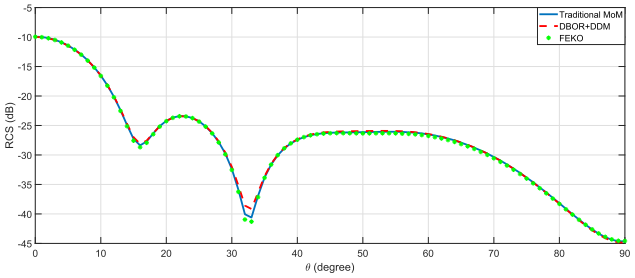

FIGURE 24. Comparison of the scattered field related to the non-DBOR microstrip FSS array at the frequency of 9.85GHz and in $\phi = 90°$ plane with V-Pole for traditional MoM (Full Structure), the DBOR method, and the obtained results from the commercial FEKO software.

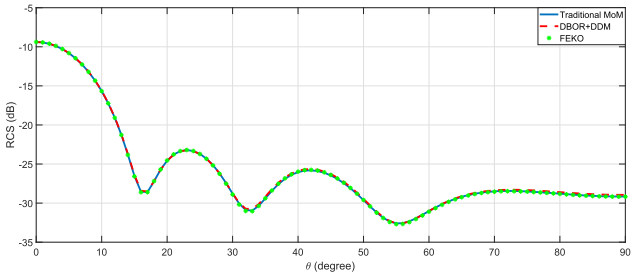

FIGURE 25. Comparison of the scattered field related to the non-DBOR microstrip FSS array at the frequency of 9.85GHz and in $\phi = 90°$ plane with H-Pole for traditional MoM (Full Structure), the DBOR method, and the obtained results from the commercial FEKO software.

memory and calculation speed compared to the traditional MoM.

Based on the two presented tables, it is evident that the necessary memory and calculation speed have significantly improved for all examples. However, further enhancements are contingent upon the choice of programming language and the approach taken in writing the code.

VI. CONCLUSION

This paper analyzed the scattered fields from various flat and cylindrical microstrip arrays using the DBOR and the DBOR+DDM methods. The simulated arrays exhibit discrete rotational symmetry throughout the entire structure or a portion of it. In cases where the structure lacks complete symmetry, we employed the DDM method to integrate symmetric and asymmetric parts. These microstrip arrays include antenna arrays, FSS absorbers, and similar structures.

The proposed method offers a distinct advantage over the traditional MoM by significantly reducing calculation time and memory requirements by factors of Ns^3 and Ns^2, respectively. However, it is essential to acknowledge that achieving these ratios is unattainable due to the inherent overhead calculations associated with implementing the proposed method. Nevertheless, the proposed method effectively minimizes calculation time and memory demands compared to the traditional MoM. Further enhancements depend on the choice of programming language and the approach taken in writing the code.

In future investigations, we will employ the proposed method to determine the radiation pattern and reflection coefficient S_{11} in the microstrip array antennas.

REFERENCES

[1] W. L. Stutzman and G. A. Thiele, *Antenna Theory and Design*, 3rd ed. Hoboken, NJ, USA: Wiley, 2013.
[2] C. A. Balanis, *Advanced Engineering Electromagnetics*, 2nd ed. Hoboken, NJ, USA: Wiley, 2012.
[3] J. F. Kiang, "Asymptotic high frequency methods," in *Novel Technologies for Microwave and Millimeter-Wave Applications*, 1st ed. New York, NY, USA: Springer, 2004, ch. 20.
[4] Dassault Systemes. *Electromagnetic Simulation Solvers*. Accessed: Aug. 2023. [Online]. Available: https://www.3ds.com/products-services/simulia/products/cst-studio-suite/solvers
[5] ALTAIR. *Electromagnetics*. Accessed: Aug. 2023. [Online]. Available: https://altair.com/electromagnetics-applications
[6] W. C. Gibson, *The Method of Moments in Electromagnetics*, 3rd ed. Boca Raton, FL, USA: CRC Press, 2022.
[7] E. Newman and P. Tulyathan, "Analysis of microstrip antennas using moment methods," *IEEE Trans. Antennas Propag.*, vol. AP-29, no. 1, pp. 47–53, Jan. 1981.

[8] T. K. Sarkar and E. Arvas, "An integral equation approach to the analysis of finite microstrip antennas: Volume/surface formulation," *IEEE Trans. Antennas Propag.*, vol. 38, no. 3, pp. 305–312, Mar. 1990.
[9] W. C. Chew, J. M. Jin, E. Michielssen, and J. Song, *Fast and Efficient Algorithms in Computational Electromagnetics*, 1st ed. Norwood, MA, USA: Artech House, 2001.
[10] S. C. Chapra and R. P. Canale, *Numerical Methods for Engineers*, 8th ed. New York, NY, USA: McGraw-Hill, 2021.
[11] O. Borries, E. JΦrgensen, and P. Meincke, "Monostatic RCS of electrically large structures using higher-order MLFMM," in *Proc. 11th Eur. Conf. Antennas Propag. (EUCAP)*, Paris, France, Mar. 2017, pp. 872–876.
[12] A. K. Skrivervik and J. R. Mosig, "Analysis of finite phase arrays of microstrip patches," *IEEE Trans. Antennas Propag.*, vol. 41, no. 8, pp. 1105–1114, Aug. 1993.
[13] D. Pozar, "Finite phased arrays of rectangular microstrip patches," *IEEE Trans. Antennas Propag.*, vol. AP-34, no. 5, pp. 658–665, May 1986.
[14] C.-F. Wang, F. Ling, and J.-M. Jin, "A fast full-wave analysis of scattering and radiation from large finite arrays of microstrip antennas," *IEEE Trans. Antennas Propag.*, vol. 46, no. 10, pp. 1467–1474, Oct. 1998.
[15] N. Yuan, T. Soon Yeo, X.-C. Nie, and L. Wei Li, "A fast analysis of scattering and radiation of large microstrip antenna arrays," *IEEE Trans. Antennas Propag.*, vol. 51, no. 9, pp. 2218–2226, Sep. 2003.
[16] W.-J. Zhao, L.-W. Li, E.-P. Li, and K. Xiao, "Analysis of radiation characteristics of conformal microstrip arrays using adaptive integral method," *IEEE Trans. Antennas Propag.*, vol. 60, no. 2, pp. 1176–1181, Feb. 2012.
[17] D. C. Ross, J. L. Volakis, and H. T. Anastassiu, "Three-dimensional edge-based finite-element analysis for discrete bodies of revolution," *IEEE Trans. Antennas Propag.*, vol. 45, no. 7, pp. 1160–1165, Jul. 1997.
[18] R. Wang and J.-M. Jin, "A finite element-boundary integral formulation for numerical simulation of scattering by discrete body-of-revolution geometries," *Electromagnetics*, vol. 27, nos. 2–3, pp. 65–86, Mar. 2007.
[19] J. Guan, S. Yan, and J.-M. Jin, "An accurate and efficient finite element-boundary integral method with GPU acceleration for 3-D electromagnetic analysis," *IEEE Trans. Antennas Propag.*, vol. 62, no. 12, pp. 6325–6336, Dec. 2014.
[20] M. A. Carr, J. L. Volakis, and D. Ross, "Acceleration of free-space discrete body of revolution codes by exploiting circulant submatrices," *IEEE Trans. Antennas Propag.*, vol. 50, no. 9, pp. 1319–1322, Sep. 2002.
[21] H. T. Anastassiu, J. L. Volakis, and D. S. Filipovic, "Integral equation modeling of cylindrically periodic scatterers in the interior of a cylindrical waveguide," *IEEE Trans. Microw. Theory Techn.*, vol. 46, no. 11, pp. 1713–1720, Nov. 1998.
[22] Z. H. Fan, Z. He, and R. S. Chen, "An efficient ACA solution for electromagnetic scattering from discrete body of revolution," *ACES*, vol. 31, no. 10, pp. 1151–1157, Oct. 2016.
[23] J. M. Jin, *Theory and Computation of Electromagnetic Fields*, 2nd ed. Hoboken, NJ, USA: Wiley, 2015.
[24] G. Cheng, Z. Fan, and R. Chen, "An efficient solution for the transient electromagnetic scattering from discrete body of revolution," *IEEE Antennas Wireless Propag. Lett.*, vol. 14, pp. 670–673, 2015.
[25] H. T. Anastassiu, N. L. Tsitsas, and P. J. Papakanellos, "Scattering analysis of discrete bodies of revolution via an efficient numerical algorithm," in *Proc. URSI Int. Symp. Electromagn. Theory*, Berlin, Germany, Aug. 2010, pp. 657–659.
[26] M. A. Carr, J. L. Volakis, and D. C. Ross, "Acceleration of moment method solutions for discrete bodies of revolution in free space," in *Proc. IEEE Antennas Propag. Soc. Int. Symp.*, Salt Lake City, UT, USA, Jul. 2000, pp. 2286–2289.
[27] Y. Saad, "Domain decomposition methods," in *Iterative Methods for Sparse Linear Systems*, 2nd ed. Philadelphia, PA, USA: SIAM, 2003, ch. 14.
[28] R. Vescovo, "Inversion of block-circulant matrices and circular array approach," *IEEE Trans. Antennas Propag.*, vol. 45, no. 10, pp. 1565–1567, Oct. 1997.
[29] S. Rao, D. Wilton, and A. Glisson, "Electromagnetic scattering by surfaces of arbitrary shape," *IEEE Trans. Antennas Propag.*, vol. AP-30, no. 3, pp. 409–418, May 1982.
[30] A. Chen, C. Yang, Z. Chen, Y. Zhang, and Y. He, "Design of multi-level sequential rotation feeding networks used for circularly polarized microstrip antenna arrays," *Int. J. Antennas Propag.*, vol. 2012, pp. 1–10, Sep. 2012.
[31] M. Agarwal and M. K. Meshram, "An approach for circuit modeling of a multiband resonators based planar metamaterial absorber," *Microw. Opt. Technol. Lett.*, vol. 63, no. 1, pp. 1–7, Jul. 2020.
[32] D. Löffler, F. Rostan, G. Gottwald, and W. Wiesbeck, "Design and measured performance of cylindrical microstrip patch antenna arrays for SDMA-applications," *Frequenz*, vol. 52, nos. 3–4, pp. 66–70, Mar. 1998.
[33] M.-H. Golbon-Haghighi, H. Saeidi-Manesh, G. Zhang, and Y. Zhang, "Pattern synthesis for the cylindrical polarimetric phased array radar (CPPAR)," *Prog. Electromagn. Res. M*, vol. 66, pp. 87–98, 2018.
[34] K. Ozden, O. M. Yucedag, and H. Kocer, "Metamaterial based broadband RF absorber at X-band," *AEU-Int. J. Electron. Commun.*, vol. 70, no. 8, pp. 1062–1070, Aug. 2016.

HOSSEIN MOHAMMADZADEH was born in Yasouj, Iran, in 1987. He received the B.Sc. degree in electrical engineering from Hakim Sabzevary University, Sabzevar, Iran, in 2009, and the M.Sc. degree from the Isfahan University of Technology (IUT), Isfahan, Iran, in 2013, where he is currently pursuing the Ph.D. degree. His research interests include electromagnetic theory, propagation and scattering theory, antenna and microwave, and numerical techniques.

ABOLGHASEM ZEIDAABADI NEZHAD (Member, IEEE) was born in Sirjan, Iran, in 1961. He received the B.Sc. degree in electrical engineering from the Shahid Bahonar University of Kerman, Kerman, Iran, in 1988, and the M.Sc. and Ph.D. degrees in electrical engineering from the Sharif University of Technology, Tehran, Iran, in 1991 and 1997, respectively. Since 1997, he has been a Professor with the Department of Electrical and Computer Engineering, Isfahan University of Technology, Isfahan, Iran. He is the author or coauthor of more than 100 papers in journals and conference proceedings. His research interests include propagation and scattering theory, antenna design, active and passive microwave circuits, and semiconductor devices.

ZAKER HOSSEIN FIROUZEH was born in Isfahan, Iran, in 1977. He received the B.Sc. degree in electrical engineering from the Isfahan University of Technology (IUT), Isfahan, in 1999, and the M.Sc. and Ph.D. degrees in electrical engineering from the Amirkabir University of Technology (AUT), Tehran, Iran, in 2002 and 2011, respectively. From 2002 to 2006, he was a Research Engineer with the Information Communication Technology Institute (ICTI), IUT, where he is currently a Faculty Member with the Department of Electrical and Computer Engineering. He is experienced in designing and implementing antenna, radar, and wireless communication systems. He is the author or coauthor of more than 100 papers in journals and conference proceedings. His current research interests include antenna design and measurements, numerical techniques in electromagnetic, wave propagation and scattering, and EMC/EMI.